Indian Journal of Pure & Applied Physics
Vol. 60, September 2022, pp. 742-753
DOI: 10.56042/ijpap.v60i9.62368

Influence of Calcium Substitution on Structural, Vibrational and Paramagnetic Properties of Magnesium Ferrite

Gurbinder Kour[a], Balwinder Kaur[b]*, Ajay Singh[c], Anju Kumari[d] & Manju Arora[e]

[a]GGHSS, Mubarak Mandi, Panjtirthi, Jammu, Jammu & Kashmir-180 001, India
[b]Govt. Degree College, R.S. Pura, Jammu & Kashmir-181 102, India
[c]G. G. M. Science College, Canal Road, Jammu-Tawi, Jammu & Kashmir-180 001, India
[d]Govt. Degree College, Khour, Akhnoor, Jammu & Kashmir-181 203, India
[e]CSIR-National Physical Laboratory, Dr. K.S. Krishnan Marg, New Delhi-110 012, India

Received 15 April 2022; accepted 17 August 2022

The environment friendly calcium substituted magnesium ferrite with composition $MgCa_xFe_{2-x}O_4$ (x = 0.00, 0.01, 0.03, 0.05, 0.07) synthesized by the conventional solid – state reaction powdered samples are studied for structural, vibrational and spin characteristics for chemical sensor application. XRD patterns with Rietveld refinement reveal partial inverse spinel structure of the prepared samples with tentative cation occupancy. The rietveld refinement is performed to know the cation occupancy in the prepared samples which could be further helpful to exploit these ferrite materials for different technological applications. The intensity of ν Fe^{3+}-O stretching vibrational peaks arising from tetrahedral (ν_1) and octahedral (ν_2) sites in IR transmittance spectra are composition and cation distribution sensitive. The presence of Ca^{2+}/Mg^{2+}/Fe^{2+} ions is evidenced by the splitting of bands and shoulder peaks in IR transmittance spectra. The strong dipolar-dipolar interactions encourage broad asymmetric EPR derivative signal of Fe^{3+} ions. The substitution of diamagnetic Ca^{2+} dopant ions in lattice strengthens dipolar-dipolar interactions, broadens the resonance signal and higher g-values due to spin disorder (spin frustration).

Keywords: Solid state reaction; Crystal structure; X - ray diffraction; Electron paramagnetic resonance

1 Introduction

Magnesium ferrite and its doped analogues have been explored for usage in various technological applications like hyperthermia treatment, catalyst and humidity sensor, information storage systems, microwave devices, magnetic recording media, green anode materials and electronics etc.[1–4] due to its inherent high permeability, moderate permittivity, high resistivity and low eddy current loss properties[5,6]. These properties can be easily tailored as per application demand by optimizing the cation distribution of dopant ions at octahedral and tetrahedral sites of the spinel lattice. The cation distribution provides vital information in predicting the crystalline and electronic structural details of the ferrites under study and their effect on electrical, catalytic, optical and magnetic properties. The cation distribution in spinel lattice is till today an attractive and challenging problem for researchers though the work has been going on from about last five decades.

*Corresponding authors: (Email: bkaur77@gmail.com)

The spinel unit cell of MFe_2O_4 general formula is face centered cubic lattice which consists of 64 tetrahedral interstitial sites and 32 octahedral sites, out of which 8 tetrahedral and 16 octahedral sites are occupied by cations and belongs to $Fd\bar{3}m$ (O_h^7) space group. The cations, and anions acquire (8a and 16d) and anions 32e positions respectively and oxygen parameter is designated by 'u' in oxide spinels[7]. The general structural formula of Mg doped ferrite is given as $(Mg_{1-x}Fe_x)[Mg_xFe_{2-x}]O_4$, where x represents the degree of inversion (defined as the fraction of (A) sites occupied by Fe^{3+} ions) and presents normal state, inverse state or mixed state when x=0, 1 and $0 < x < 1$ respectively as per the distribution of cations on (A) and [B] sites[8]. The overall properties of spinel ferrites pertain to the distribution of cations at [A] and [B] sites. The cation distribution studies of slowly cooled Mg – ferrite (i.e., from 1773 K to room temperature) reported[9] the nearly inverse spinel lattice for x = 0.9 composition, and also depends upon the selection of synthesis process[10].

The distribution of cations between octahedral and tetrahedral sites in the spinel structure helps in the

optimization of desired physical, electrical and magnetic properties as per device requirement. The cation distribution in ferrites lattice depends upon the electronic configuration, valency and ionic radius of the dopant/co-dopant ions[11] present at (A) and [B] sites. X-ray diffraction, Neutron diffraction, IR, EPR, NMR, Mossbauer analytical techniques have been used for the structure and paramagnetic properties characterization as well as cations distribution at non-equivalent crystallographic positions. The extensive work on doping/substitution of spinel ferrites by magnetic and non – magnetic ions have been reported to optimize lattice parameters, electrical and magnetic properties [6, 12–18]. The structural and magnetic characteristics of $MgFe_2O_4$ with non – magnetic ions substitution e.g. Zn^{2+} [6, 19], Ca^{2+} [20 – 22], Ti^{4+} [23], Zr^{4+} [24], Al^{3+} [9, 25], Dy^{3+} [26, 27] and Cr^{3+} [15] were investigated by X – ray diffraction (XRD) and magnetic measurement techniques.

Chhaya et al[21] studied the dopant ions substitution limit, structural, bulk magnetic and electrical properties of Ca^{2+} substituted magnesium ferrite and found that a maximum of 23% of Ca^{2+} can be accommodated for Mg^{2+}. The cation distribution is explored from the XRD intensity analysis for the separated fcc spinel phase by the comparison of calculated while, the observed XRD intensity revealed the substitution limit and the percentage of fcc phase formation. Nanocrystalline Mg – ferrite powders have been prepared by high energy ball milling having stoichiometric mixture of MgO and α-Fe_2O_3 powders[8]. Analysis of 9 hour ball – milled nanocrystalline Mg – ferrite samples by Rietveld's method showed the presence of mixed and nearly inverse spinel as major and minor phases, respectively, along with ~3 wt% of unreacted α-Fe_2O_3. The distribution of cations at (A) and [B] sites in mixed spinel matrix varies continuously, while occupancy of Fe^{3+} ions at (A) site (inverse spinel) increases with increasing annealing temperature. The quantitative analysis of the XRD data evaluated on the basis of Rietveld structure refinement method yields detailed insight about the structure and microstructure of synthesized nanoscale $NiAl_xFe_{2-x}O_4$ ferrite[17]. The cation distribution data of this work suggests Al^{3+} ions preferentially substitute at octahedral [B] site and Ni^{2+} ions migrate to tetrahedral site.

Waldron[28] reported IR transmittance studies of several ferrites and assigned ν Fe^{3+}-O stretching vibrations at tetrahedral and octahedral sites. Srivastava and Srinivasan[29] investigated IR spectra of MFe_2O_4 (M = Mn, Fe, Co, Ni, Cu and Zn) ferrites at room temperature in 1000-200 cm^{-1} range. The researchers have also reported the work on IR studies of various ferrites doped with non-magnetic metal ions e.g. Zn^{2+} [30], Cd^{2+} [31], Li^{+} [32], Ti^{4+} [33]. EPR studies were reported on cobalt substituted Nickel ferrite[34], cadmium[35] and praseodymium[36] substituted magnesium ferrites. The considerable work has been going on the variations in physical properties in non-magnetic ions substituted pure and mixed ferrites[37].

The substitution of magnetic and non – magnetic ions affect the overall properties of ferrites due to their accommodation ability and distribution at tetrahedral (A) and octahedral [B] sites. In the present work, $MgCa_xFe_{2-x}O_4$ (where x = 0.00, 0.01, 0.03, 0.05, 0.07) powdered samples were prepared by solid state reaction technique. The ionic radii of Mg^{2+}, Ca^{2+}, and Fe^{3+} cations are 0.66 Å, 0.99 Å and 0.64 Å respectively. These studies are quite interesting due to the substitution of larger Ca^{2+} ions at Fe^{3+} site in $MgFe_2O_4$. Earlier, we reported the synthesis, structural and magnetic characteristics of Ca doped magnesium ferrite[22]. X-ray diffraction patterns confirm the formation of cubic spinel structure. The lattice parameter increases up to $x \leq 0.03$ and then decreases for $x > 0.03$. EDAX data confirm the desired elemental stoichiometry composition of the prepared samples and discussed the decrease in grain size with increase in Ca^{2+} content. The magnetic characteristic exhibits the soft ferromagnetic nature of the as prepared samples. The magnetization increases for small Ca concentration i.e, $x \leq 0.05$, and then decreases on further increasing Ca concentration; that is, $x > 0.05$. Pure Mg – ferrite has the highest curie temperature and reduces on increasing Ca^{2+} ions concentration[22]. Ca^{2+} ions prefer acquiring tetrahedral sites of the spinel lattice[21, 38]. Till date, to the best of our knowledge, the detailed investigations on IR and electron paramagnetic resonance (EPR) studies of Ca^{2+} doped magnesium ferrite are not reported so far. The main aim of this research is to perform Rietveld refinement for structural analysis, FTIR and EPR studies of Ca^{2+} ions doped $MgFe_2O_4$, to infer the cations distribution in crystallographic sub-lattices at octahedral and tetrahedral sites. These studies reflect dopant/substituent and the synthesis parameters sensitive spinel ferrites properties and helps in using them as sensing electrode in chemical sensor application in near future.

2 Materials and Methods

2.1 Materials preparation

The polycrystalline calcium substituted magnesium ferrite having the compositional formulae $MgCa_xFe_{2-x}O_4$ (where x = 0.00, 0.01, 0.03, 0.05, 0.07) were prepared using the conventional solid-state reaction method. High purity analytical grade MgO, Fe_2O_3, CaO were used in stoichiometric proportion by weight. The solid-state reaction was carried out in muffle furnace maintained at 800 °C for 2 hours with a heating rate of 2 °C/min for the initial chemical reaction between the starting materials. The pre-sintered mixture was ground to fine powder and pressed into the circular/rectangular shaped pellets by using hydraulic press under a pressure of 120 kg/cm^2 to obtain a high degree of compaction. In the final sintering process, the samples were placed in a furnace heated upto 1200 °C with a heating rate of 4 °C/min, kept for 2 hours, cooled to 900 °C at the rate of 7.5 °C/min and then cooled to room temperature. After sintering, the pellets were polished to remove the surface layers by ensuring that the measured properties are of the bulk sample and not the surface layers[22].

2.2 Characterization

Infrared transmission spectra were recorded on Perkin Elmer's IR spectrometer (Model No. 70768) using sample in KBr pellet form in 4000 – 400 cm^{-1} region at ambient temperature. Electron paramagnetic resonance spectra were recorded on Bruker Biospin A300 X-band EPR spectrometer. DPPH (1,1-diphenyl 2–picryl hydrazyl) was used as a standard field marker for g – value and spin concentration calculations. These spectra were recorded in magnetic field 4000 $\pm$ 4000 G range at 9.26 GHz microwave frequency, 23 db microwave power and 100 kHz modulation frequency.

3. Results and Discussion

3.1 Structural Characterization

XRD studies of $MgCa_xFe_{2-x}O_4$ (where x = 0.00, 0.01, 0.03, 0.05, 0.07) samples confirm the formation of polycrystalline cubic spinel phase[22]. A typical peak at 37° (222) is observed in all compositions pertaining to MgO (JCPDS Card No: 78-0430). All XRD patterns were analyzed using the computer program FullProf 2K (version 4.30 – Apr 2008 – ILL JRC) in the Rietveld method for structure refinement. The peaks shape in the experimental diffraction patterns was described by an asymmetric pseudo – Voigt (pV) function. The background of each pattern was fitted by a polynomial function of degree 5. Program refinement was performed with the $Fd\bar{3}m$ space group, origin at $\bar{3}m$, O^{2-} in 32e, A – site in 8b and B – site in 16c. The quality of Rietveld fitting was tested by using the reliability R – factors: expected $R_{exp.}$, Bragg R_{Bragg}, profile R_P and weighted profile R_{WP} (weighted difference between measured and calculated values) should be less than 10% as well as the goodness of fit (GOF = R_{WP}/ $R_{exp.}$) must be near to one.

The Rietveld refinement performed on X – ray diffraction patterns of all the compositions at room temperature are shown in Fig. 1(a) – (e). The graphs contain experimental and calculated data along with the difference between the two. The data was processed on the FullProf program for structure refinement and continued till convergence reached at the value of the quality factor i.e. GoF close to 1 (varies between 1.0 to 1.6), for the confirmation of goodness of refinement. The values of discrepancy factor and expected values with goodness of fit index are listed in Table 1(a). The cation distribution was derived from FullProf program[39]. $MgFe_2O_4$ is basically a partially inverse spinel ferrite[22, 40] and considered as collinear ferrimagnet whose degree of inversion is very sensitive to sample preparation route. Fig. 2(a) and 2(b) presents the unit cell of pure and 5% Ca doped Magnesium ferrite respectively. Fig. 2(c) exhibits the unit cell of 5% Ca doped in the polyhedrons form with tetrahedral and octahedral sites. In Fig. 2(a), Mg^{2+} and Fe^{3+} ions are represented by the blue and green colored balls respectively, present at both the tetrahedral (A) as well as octahedral [B] interstitial sites. It means that the prepared magnesium ferrite is partially inverse spinel ferrite. The ionic radii of Mg^{2+}, Ca^{2+} and Fe^{3+} cations are 0.66 Å, 0.99 Å, 0.64 Å respectively. So, it is quite interesting to explore the substitution of large cation Ca^{2+} for Fe^{3+} in $MgFe_2O_4$. While Fig. 2(b) shows that Ca^{2+} ions acquire octahedral sites instead of tetrahedral. Ca^{2+} ions occupancy at the octahedral site is represented by the pink colored ball in the Fig. 2(b). The white color at the octahedral site reveals the existence of voids created by the doping of Ca^{2+} ions at the octahedral sites. In spinel ferrites, mostly the radius of ions present at octahedral site have larger radius than at the tetrahedral site. So smaller ions prefer tetrahedral sites. Also, the trivalent ions are

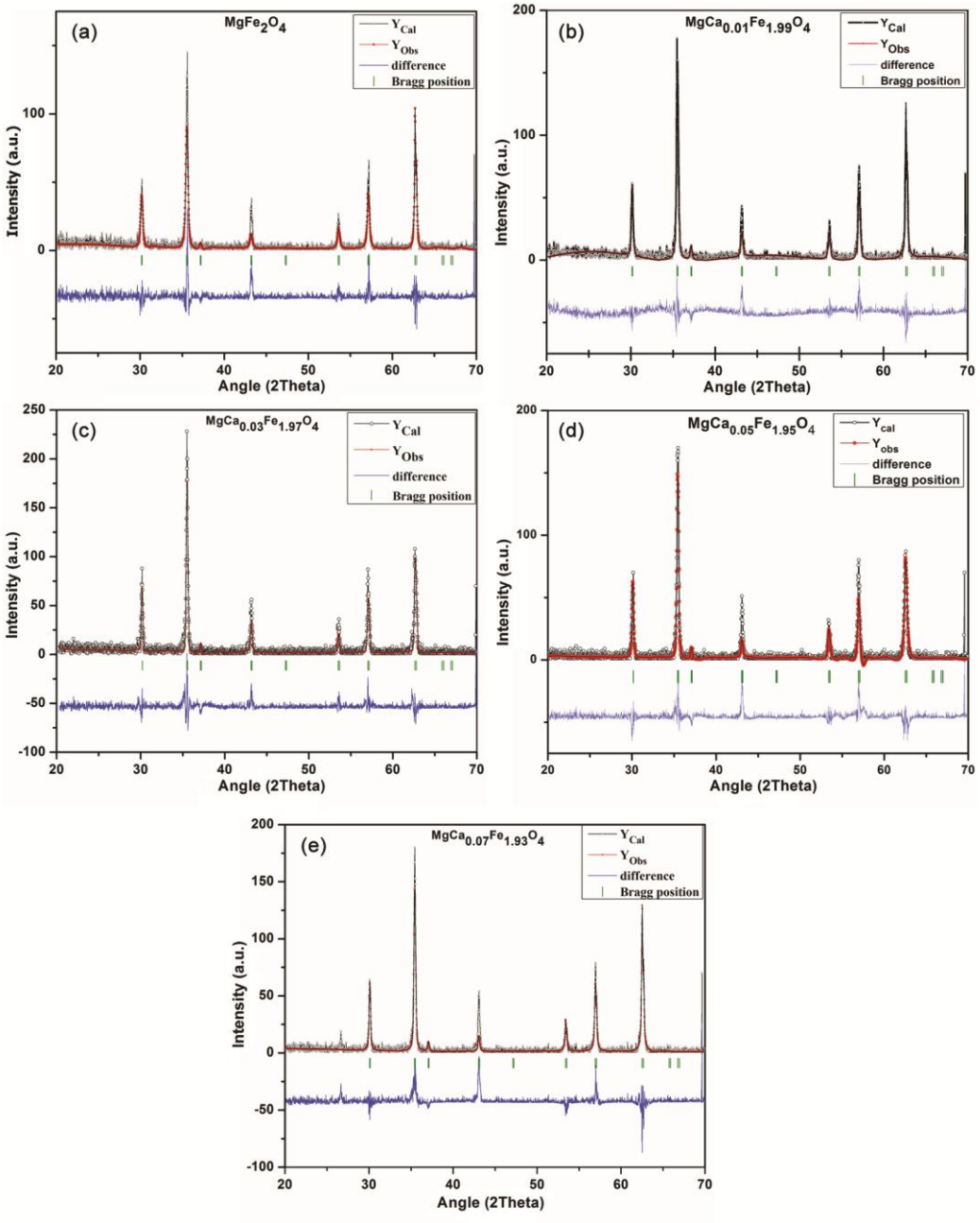

Fig. 1 — Rietveld refined XRD patterns for $MgCa_xFe_{2-x}O_4$ (x = 0.0, 0.01, 0.03, 0.05, 0.07).

Table 1(a) — Rietveld agreement factors, lattice constant, and unit cell volume of pure and Ca doped Magnesium ferrite

Composition	R_P (%)	R_{wp} (%)	$R_{exp.}$ (%)	χ^2	a=b=c (Å)	V (Å^3)
MgF	5.87	5.95	5.35	1.23	8.3719	586.78
Ca1%	5.41	5.52	5.26	1.10	8.3801	588.50
Ca3%	5.73	5.83	5.28	1.22	8.3819	588.88
Ca5%	4.31	4.84	4.76	1.03	8.3976	592.20
Ca7%	5.55	5.65	5.31	1.13	8.3975	592.17

(*Contd.*)

Table 1(b) — Lattice parameters and density calculated using XRD and Rietveld method for $MgCa_xFe_{2-x}O_4$ (x = 0.0, 0.01, 0.03, 0.05, 0.07) (*Contd*.)

Composition	XRD		Rietveld	
	Lattice parameters (Å)	Density (gm/cm^3)	Lattice parameters (Å)	Density (gm/cm^3)
MgF	8.3848	4.5062	8.3719	4.5238
Ca1%	8.4108	4.4610	8.3801	4.5096
Ca3%	8.4405	4.4071	8.3819	4.5005
Ca5%	8.4211	4.4783	8.3976	4.4675
Ca7%	8.4046	4.4721	8.3975	4.4828

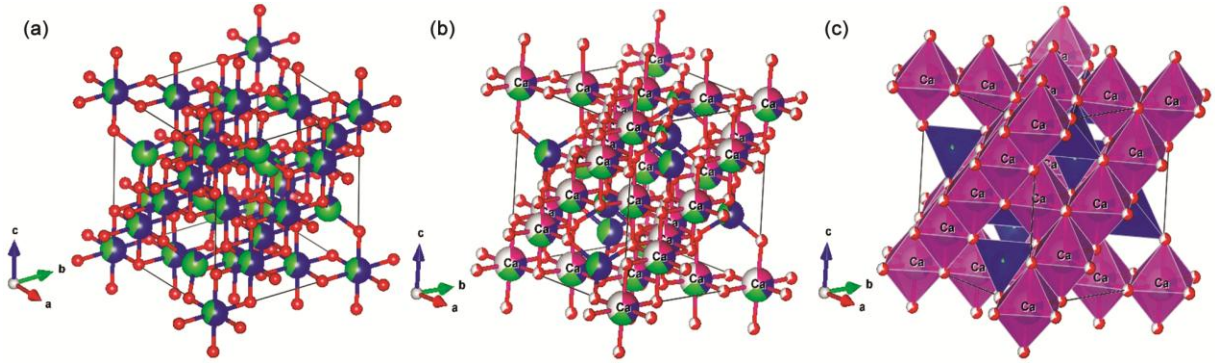

Fig. 2 — (a) Unit cell showing the partial inverse structure in pure magnesium ferrite. Mg^{2+} (blue colour) and Fe^{3+} (green colour) cations present at both the tetrahedral as well as octahedral sites. (b) Unit cell showing the occupation of Ca^{2+} ions (pink colour) at octahedral sites in 5% Ca^{2+} ions doped magnesium ferrite. (c) Unit cell of 5% Ca^{2+} ions doped magnesium ferrite showing tetrahedral sites (in blue colour) and octahedral site (in purple colour) in the form of Polyhedra.

smaller than the divalent ions and favor the inverse structure[7]. The occupancy of Ca^{2+} ions with large ionic radius (0.99 Å) prefer the octahedral sites in the present substituted compositions of magnesium ferrite. It was reported in some studies that at low doping level Ca^{2+} ions acquire tetrahedral sites and at higher concentrations substitute at octahedral sites[21, 38]. In the present case, Ca^{2+} ions occupy octahedral sites in all the compositions.

The values of lattice parameters and X – ray density calculated from XRD patterns and Rietveld refined method for all compositions of pure and Ca doped magnesium ferrite are calculated and tabulated in Table 1(b). The values of cell parameters derived by Rietveld refinement shows an increase with Ca^{2+} ions doping concentration follows Vegard's law while density reduces on increasing Ca^{2+} ions concentration. The increase in the values of lattice parameters is attributed to large ionic radius of Ca^{2+} ions substituting the ions present at octahedral sites. Table 2(a) and 2(b) show the atomic coordinates, occupancy and multiplicity of different atoms in pure Mg – ferrite and 5% Ca doped Mg – ferrite respectively obtained from Rietveld refinement.

3.1.1 Cation Distribution

The precise spinel structural details of ferrites are the basis for cation distribution theories[41, 42]. The spinel unit cell is face-centered cubic structure having cations at 8a and 16d positions and anions at 32e positions.

The simple oxide spinel belongs to AB_2O_4 stoichiometry having A and B cations with formal charges desired for charge neutrality condition:

$$Q_A+2Q_B + 4Q_O = 0 \quad \ldots (1)$$

where Q_A and Q_B are the charges on A and B cations, and Q_O of anions (-2 for oxide spinels). In 2 – 3 and 4 – 2 spinel lattices, A = 2 and B = 3 and A = 4 and B = 2 respectively. In normal spinel AB_2O_4 lattice, A cation occupies the tetrahedral site, and two B cations at the two equivalent octahedral sites. Barth and Posnjak[43] reported first time in $MgAl_2O_3$ the alternative perfectly inverse distribution $(B)[AB]O_4$ arrangement. In all spinel lattices, the cations distribution fall between these two extremes i.e. from normal spinel to inverse spinel lattice by considering an additional parameter, the degree of inversion (δ) which is the fraction of tetrahedral sites occupied by

Table 2(a) — Typical atomic coordinates (x, y, z) of different atoms for pure Mg – Ferrite

Atom	Chem	x	Y	z	Occupancy	Multiplicity
Mg	MG	0.3750	0.3750	0.3750	0.0063	8
Fe	FE	0.3750	0.3750	0.3750	0.0354	8
Mg	MG	0.0000	0.0000	0.0000	0.0492	16
Fe	FE	0.0000	0.0000	0.0000	0.0406	16
O	O	0.2459	0.2459	0.2459	0.230	32

Table 2(b) —Typical atomic coordinates (x, y, z) of different atoms for 5% Ca doped Mg – Ferrite

Atom	Chem	X	Y	Z	Occupancy	Multiplicity
Mg	MG	0.3750	0.3750	0.3750	0.0192	8
Fe	FE	0.3750	0.3750	0.3750	0.0225	8
Mg	MG	0.0000	0.0000	0.0000	0.0169	16
Fe	FE	0.0000	0.0000	0.0000	0.0436	16
Ca	CA	0.0000	0.0000	0.0000	0.0053	16
O	O	0.236	0.236	0.236	0.1371	32

Table 3(a) — Cation Distribution of $MgCa_xFe_{2-x}O_4$ (x = 0.0, 0.01, 0.03, 0.05, 0.07)

Composition (x)	Cation Distribution		Oxygen parameter U	Inversion parameter (δ)
	A – site	B – site		
0.0	$Mg_{0.006}\ Fe_{0.964}$	$Mg_{0.951}\ Fe_{1.041}$	0.3852	0.0102
0.01	$Mg_{0.025}\ Fe_{0.983}$	$Mg_{0.982}\ Fe_{1.01}\ Ca_{0.0152}$	0.3851	0.0101
0.03	$Mg_{0.0195}\ Fe_{0.978}$	$Mg_{0.994}\ Fe_{1.03}\ Ca_{0.001}$	0.3850	0.010
0.05	$Mg_{0.019}\ Fe_{0.978}$	$Mg_{0.983}\ Fe_{1.038}\ Ca_{0.0053}$	0.38478	0.00978
0.07	$Mg_{0.014}\ Fe_{0.972}$	$Mg_{0.979}\ Fe_{1.037}\ Ca_{0.0136}$	0.38477	0.00977

Table 3(b) — Values calculated for Tetrahedral (r_A) and Octahedral (r_B) ionic radii, Tetrahedral (R_A) and Octahedral (R_B) site radius

Composition (x)	r_A	r_B	Rietveld method		Theoretical values	
			R_A	R_B	R_A	R_B
0.0	0.6401	0.6495	1.872	2.059	1.9601	2.011
0.01	0.6405	0.6525	1.901	2.046	1.9604	2.014
0.03	0.6404	0.6500	1.816	2.095	1.9602	2.015
0.05	0.6404	0.6506	2.02	1.989	1.9603	2.020
0.07	0.6403	0.6520	1.92	2.042	1.9602	2.020

B ions. δ varies between 0 and 1 for the perfect normal and inverse spinel structures respectively. As a special case $(A_{1/3}B_{2/3})\ [A_{2/3}B_{4/3}]O_4$ represents the completely random arrangement.

As we know that A site is smaller than the B sites and are not able to accommodate available cations without local distortion of the sites. Thus, each A site expands by an equal displacement of the four surrounding oxygen ions, towards and along the body diagonal of cube, to form a tetrahedral with A – cation having cubic symmetry. However, six oxygen ions surrounding a B site are shifted in such a way that this oxygen octahedral shifts by the same amount, as the first expands. A quantitative measure of this displacement is the oxygen positional parameter (u), given by a distance between an oxygen ion and a face of a cube. The ideal value of this FCC parameter is u = 0.375. The u value for spinel ferrite ranges between 0.375 and 0.385[16]. The average values of the tetrahedral (r_A) and octahedral (r_B) ionic radii for each composition have been estimated. The value of oxygen positional parameter (u) was also calculated in order to find the values of bond lengths of tetrahedral (R_A) and octahedral (R_B) sites. The different formulae used to calculate these parameters are taken from the reported literature[16] and these values are listed in Table 3 (a) and 3 (b).

3.2 Spectroscopic properties

3.2.1 Fourier transform infrared spectroscopy (FT-IR)

IR spectroscopy is one of extensively used non-destructive fast technique for materials characterization by the researchers to reveal the vibrational and structural properties of materials.

$MgFe_2O_4$ spinel ferrite belongs to $Fd\bar{3}m$ space group and its normal modes of vibrations [44] are given as:

$$A_{1g}(R) + E_g(R) + F_{1g} + 3F_{2g}(R) + 2A_{2u} + 2E_u + 4F_{1u}(IR) + 2F_{2u} \quad \ldots (1)$$

Where A_{1g}, Eg and $3F_{2g}$ are the five Raman active, $4F_{1u}$ are IR active and remaining six $2A_{2u}$, $2E_u$ and $2F_{2u}$ are forbidden modes. These vibrations arise from the motion of O ions with A – site and B – site ions in the spinel structure[45]. While, F_{1u} mode results from asymmetric stretching vibration of oxygen anion with respect to A-site and B-site cations

FTIR spectra of the $MgCa_xFe_{2-x}O_4$ ferrite system (For x = 0.00, 0.01, 0.03, 0.05, 0.07) are shown in Fig. 3 (a), (b), (c), (d) and (e) respectively. The ν_1 and ν_2 transmission peaks correspond to intrinsic lattice vibrations of octahedral and tetrahedral bonding groups in the spinel structure respectively. The difference in frequency between the characteristic vibrations ν_1 and ν_2 modes is attributed to the long bond length of oxygen - metal ions in the tetrahedral groups. Using the values of ν_1 and ν_2, force constants (K_T and K_O) were computed.

The force constants (K) for the tetrahedral site (K_T) and octahedral site (K_O) are calculated using the following relation[46]

$$K = 4\pi^2 c^2 \nu^2 m \quad \ldots (2)$$

where 'c' is the velocity of light ~ 2.99×10^{10} cm sec^{-1}; 'ν' is the vibration frequency of the tetrahedral and octahedral sites; 'm' is the reduced mass for the Fe^{2+} ions and the O^{2-} ions, it is found equal to ~ 2.061×10^{-23} gm.

Force constants for metal oxygen bonds present in tetrahedral (K_T) and octahedral (K_O) sites can also be obtained using the following relations:

$$K_T = 7.62 \times M_A \times v_1^2 \times 10^{-3} \quad \ldots (3)$$

$$K_O = 10.62 \times \frac{M_B}{2} \times v_2^2 \times 10^{-3} \quad \ldots (4)$$

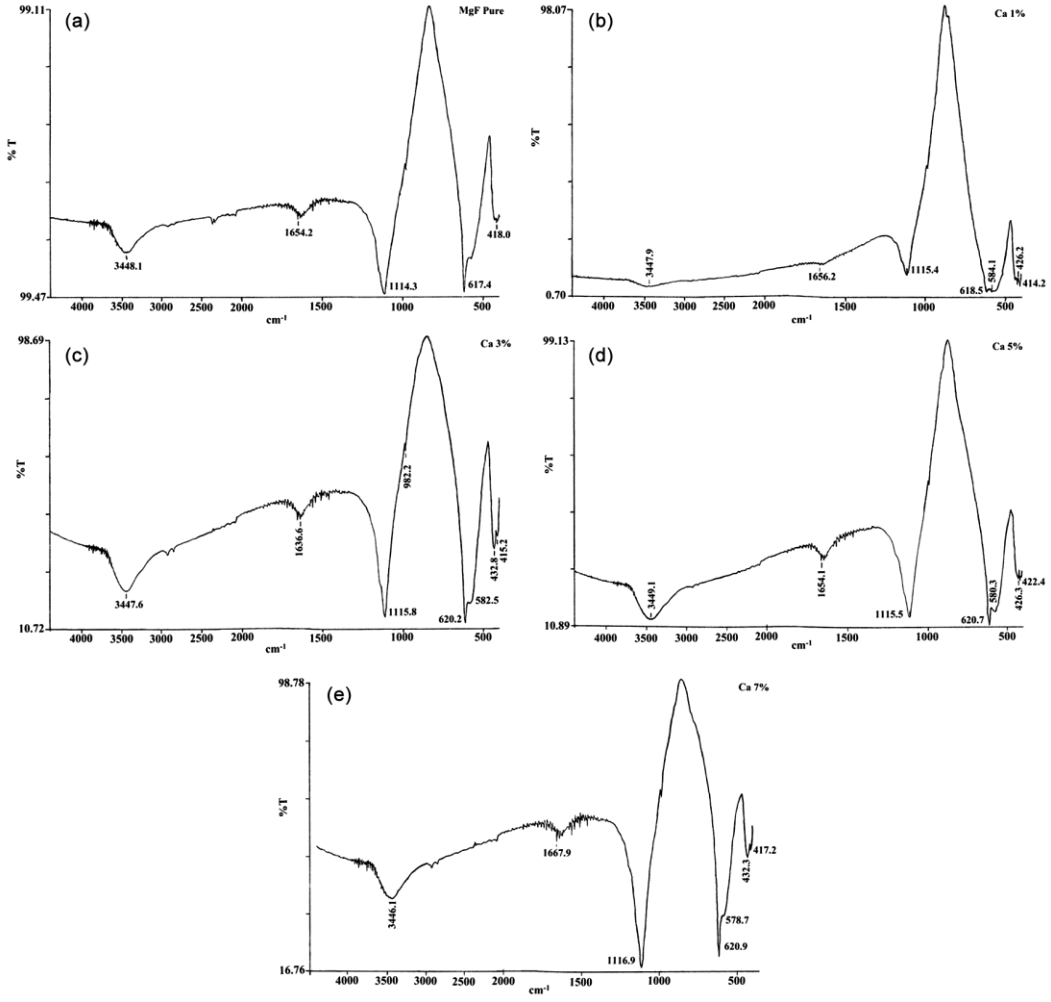

Fig. 3 — FTIR spectras for $MgCa_xFe_{2-x}O_4$ (where x = 0.00, 0.01, 0.03, 0.05, 0.07).

Table 4 — Position of IR absorption bands (ν_1, ν_2) and force constants for tetrahedral and octahedral (F_T, F_O) in case of $MgCa_xFe_{2-x}O4$ system (x = 0.0, 0.01, 0.03, 0.05, 0.07)

Content (x)	ν_1 (cm^{-1})	ν_2 (cm^{-1})	$F_T \times 10^5$ (dynes/cm)	$F_O \times 10^5$ (dynes/cm)
0.00	617.4	418	2.788	1.278
0.01	618.5	426.2	2.798	1.291
0.03	620.2	432.8	2.813	1.315
0.05	620.7	426.3	2.818	1.317
0.07	620.9	432.3	2.820	1.319

The values of ν_1 and ν_2 and K_T and K_O are given in Table 4 as calculated from equation (2)[47].

Table 4 contains the compiled data of IR transmission bands peak position (ν_1, ν_2) and force constant (K_T, K_O) for tetrahedral and octahedral site as a function of x. To study the compositional dependence of force constants, K_T and K_O are plotted with calcium concentration (x) as shown in Fig. 4 and both K_T and K_O increases with x. The shifting of ν_1 mode towards higher frequency indicates the increase in 'K_T' force constant due to the increase in strong bonding between the oxygen ions and metal ion at the A – sites. While, increase in force constant for octahedral site 'K_O' with 'x' suggests the strengthening of interatomic bonding between the anions and B – site cations. Table 4 shows $K_T > K_O$ which confirms the band frequency associated with tetrahedral sites is more than that for octahedral sites.

IR transmission spectra of $MgCa_xFe_{2-x}O_4$ system with x = 0.00, 0.01, 0.03, 0.05 and 0.07 are presented in Fig. 3(a – e). IR transmission bands appear due to the stretching vibrations of the oxygen ions linked cations bonds in the ferrite lattice. The partially inverse structure of $MgFe_2O_4$ causes broadening of peaks and weak inter-molecular coupling, shifts peak position to either higher or lower wave number with the change in intensity. The intensity of the IR peak reveals the change in electric dipole moment with inter-atomic distance. In Fig. 3 (a – e), IR transmission spectra of pure and calcium doped magnesium ferrite shows two major absorption bands below 1000 cm^{-1}, common feature for all the ferrites[28]. The high frequency ν_1 band is in the range of 617 – 621 cm^{-1} and the lower frequency band ν_2 is in the range of 418 – 433 cm^{-1}. The asymmetric stretching vibrations of the metal - oxygen bond ν_1 mode corresponds to tetrahedral site (T_d) (A – site) and ν_2 of octahedral site (O_h) (B – site) and their peak positions are composition dependent. The difference in band positions is attributed to difference in the Fe-O distances i.e. force constants for the octahedral and tetrahedral complexes. It was found that the distance between Fe^{3+}-O^{2-} ions at A – site (1.87 Å) is smaller than that of at the B – site (2.06 Å) which indicates the inverse relationship of peak position with the bond length. This may be due to more covalent nature of Fe^{3+} ions at the A – sites than at the B – sites[31].

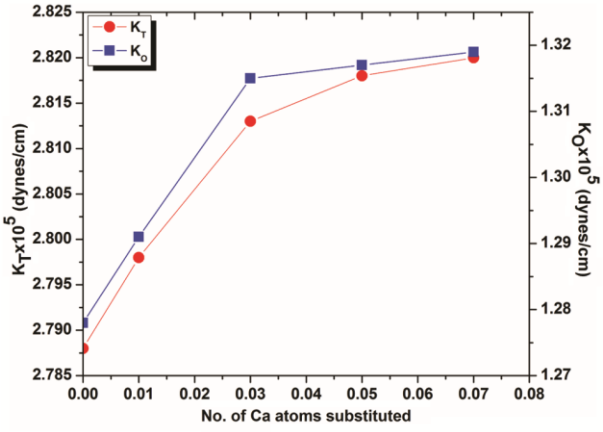

Fig. 4 — Variation of force constant for tetrahedral sites and octahedral sites with Ca composition.

The ν_1 peak shifts towards high frequency with increasing Ca^{2+} ion doping concentration. In mixed spinel ferrite materials, when the concentration of divalent metal ions increases, it brings structural changes due to cation distribution in the spinel crystal lattice and lattice vibrations[45]. ν_1 exhibits removal of degeneracy and appearance of shoulder with increasing calcium concentration (x) owing to ordering of cations[48]. The shift in ν_1 peak position is attributed to the charge imbalance at A – sites resulted from the shifting of oxygen ions slightly towards Ca^{2+} ions and the distortion of Ca^{2+} - O^{2-} tetrahedron perturbs the Fe^{3+}-O^{2-} linkages. The substitution of bigger size Ca^{2+} ions at Fe^{3+} ions at B – site causes firmness of Ca^{2+} ions at B-sites and explains the increase in lattice parameter value[49]. The vibrational peak of this mode appears at higher wavenumber due to decrease in Fe – O bond length[31]. The appearance of shoulder / splitting of ν_1 band shows Jahn - Teller distortion produced by the Fe^{2+} ions. This distortion causes local deformation in the spinel lattice owing to non – cubic component of the crystal field potential and splitting of ν_1 band[49].

The strong ν_2 mode is slightly shifted towards higher frequency with Ca^{2+} ions doping upto $x \geq 0.05$, and then it remains more or less constant. This confirms the occupation of Ca^{2+} ions at octahedral

site[50, 51] and the reason behind the increase in lattice parameter. Further, the splitting of ν_2 absorption band confirms the presence of cations of different characters at the same site[48].

In addition to these stretching vibrations, free adsorbed water stretching and bending transmission modes appear in the range from 3445 – 3450 cm^{-1} and 1635 – 1668 cm^{-1} in these IR transmission spectra of these samples.

3.2.2 Electron Paramagnetic Resonance (EPR)

Electron Paramagnetic resonance (EPR) is a very sensitive and sophisticated non-destructive spectroscopic technique used for the detection of one or more unpaired electrons present in a material qualitatively and quantitatively from ppm to ppb level. EPR spectrum is obtained by scanning the magnetic field (H) range at microwave frequency (ν). The resonance field value of EPR line depends on the ratio of H to ν and the effective gyromagnetic factor (g). The g – value is determined from the following equation:

$$g = \frac{h\nu}{\beta H} \quad \ldots (5)$$

where h is Planck's constant, ν is the microwave frequency, H (resonance field) is the magnetic field occurring at the maximum derivative resonance signal and β is the Bohr magnetron. The g-value is a function of the molecular motion, the spin properties and the symmetry of ions. The free isolated electron has g-value 2.0023 and this value deviates from free electron g-value in materials due to involvement of different interaction among with and within magnetic grains.

The dipolar-dipolar interactions and super-exchange interactions between the magnetic ions through oxygen ions are the two predominant interactions in ferrites which influence the g – value, spins concentration and the resonance peak-to-peak line width (ΔH_{pp}) parameters. The strong dipolar-dipolar interactions among magnetic grains results broad absorption signal while dominance of super-exchange interactions produce a narrow resonance line signal. A broad, symmetric EPR spectrum recorded at ambient temperature for different Ca^{2+} ions concentration doped $MgFe_2O_4$ ferrite are shown in Fig. 5. The values of various parameters such as g-value, peak to peak line width (ΔH_{pp}), relaxation time (τ_2), spin concentration (N_s), resonance field (H_r) and signal intensity are calculated by analyzing the spectra using Lorentzian distribution function and tabulated in Table 5.

The spins can dissipate their excessive energy by spin – lattice and spin – spin two relaxation process in a material. When spins are like, the magnetic exchange interaction causes a broadening of resonance lines and a narrowing of resonance lines results from the magnetic exchange interactions taking place between unlike spins. The spin lattice relaxation process is characterized by a time constant (τ_1), which is a function of static magnetic field and depends on the rate at which microwave energy is absorbed and dissipated in a material. This relaxation time is correlated with the line width of EPR signal. While, in the spin – spin relaxation time (τ_2) constant

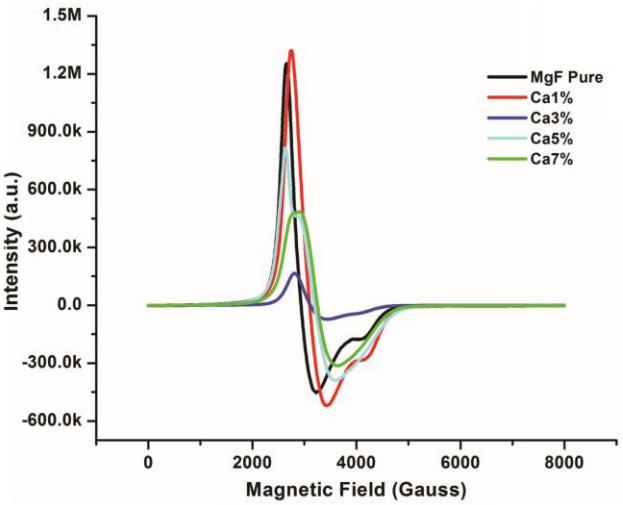

Fig. 5 — Plot showing comparison of EPR spectra of pure and Ca substituted magnesium ferrite at room temperature.

Table 5 — Peak to peak line width (ΔH_{pp}), g – value, resonance field (H_r), relaxation time (τ_2) and spin concentration (N_s) for $MgCa_xFe_{2-x}O_4$ (x = 0.0, 0.01, 0.03, 0.05, 0.07)

Sample	ΔH_{pp}	g – value	H_r	τ_2	N_s
Pure	572.6	2.41041	2658.84	9.518×10^{-15}	$5.83 \times 10^{+15}$
Ca1%	822.6	2.240559	2744.86	7.1275×10^{-15}	$7.86 \times 10^{+15}$
Ca3%	621.0	2.26425	2807.42	9.3427×10^{-15}	$9.95 \times 10^{+14}$
Ca5%	951.6	2.2094	2635.38	6.2482×10^{-15}	$6.83 \times 10^{+15}$
Ca7%	774.2	2.1727	2909.09	7.8097×10^{-15}	$4.70 \times 10^{+15}$

measures how the higher energy spin dissipates its excessive energy to neighbouring electron spin for its excitation. The value of this time constant is determined from the resonance line peak to peak line width by the following relation[52].

$$\frac{1}{\tau_2} = \frac{2\pi g \beta \Delta H 1/2}{h} \quad \ldots (6)$$

$$\Delta H_{1/2} = (3)^{1/2} \Delta H_{pp} \quad \ldots (7)$$

The intensity of EPR signal is correlated to the concentration of unpaired spins in the sample. The concentration of unpaired spins is determined by comparing the sample area under the curve to DPPH standard of known unpaired spins under the same experimental conditions and optimized parameters. The area under the absorption curve is a measure of number of spins present in a sample and its value is estimated by integrating the derivative curve[53]. All these calculated values of these parameters are listed in Table 5.

These spectra show at first the increase in peak-to-peak line width (ΔH_{pp}) upto Ca 5% substituted magnesium ferrite analogues and then decreases in Ca 7% doped composition. The broadening of EPR spectra with Ca^{2+} ions doping in pure Mg – ferrite arises from spin disorder (frustrations) resulting from antiferromagnetic interactions between the neighbouring spins in the magnetic grains[54]. Among these antiferromagnetic (dipolar) interactions, some of them effectively enhances the disorder in system. While, the shift in the resonance field value and the line broadening indicates the appearance of induced fields by exchange anisotropy in magnetic materials[55]. In addition to the broad dominating signal, a weak signal superimposed over it with g-values less than 2.0000 for bulk materials are attributed to the oxygen vacancies[56]. The formation of oxygen vacancies in these samples is correlated with the synthesis process, sintering temperature and dopant concentration in the samples. The calculated g-values for pure magnesium ferrite, Ca 1% and Ca 3% composition samples are 1.4354, 1.4340 and 1.4354 respectively. The intensity of this feature reduces on increasing calcium percentage in sample.

The g – value of pure magnesium ferrite is 2.41041 and the g-values for the Ca^{2+} ion substituted magnesium ferrite lies in the range from 2.1000 to 2.2700 i.e. higher than from free electron g-value. This variation is attributed to magneto crystalline anisotropy and inter-particle interactions which shifts resonance at higher magnetic field. However the doping of Ca^{2+} ions in magnesium ferrite reduces the exchange interaction and smaller g – value[57]. The value of resonance field is increasing with Ca^{2+} ion substitution upto Ca 3%, slightly decreases in Ca 5% and attains maximum value in Ca 7% doped composition. This shift in the resonance peak position to higher field with Ca^{2+} ions doping concentration indicates increase in easy axis alignment, decrease in effective anisotropy and inter-particle interaction, which further supports broadening of line width[58]. EPR spectra of pure and Ca^{2+} ions substituted magnesium ferrite consists of broad resonance peaks with line width ranging from 573 G for pure magnesium ferrite to 952 G for Ca 5% doped magnesium ferrite. The higher values of ΔH_{pp} and g – value EPR parameters in Ca^{2+} ions doped compositions confirms the substitution of Ca^{2+} ions at Fe^{3+} ions at tetrahedral as well as at octahedral sites and strong magnetic dipolar interactions among these particles. Ca^{2+} ions preferentially enter at tetrahedral site replacing Fe^{3+} ions for lower values of Ca^{2+} ions concentration whereas for higher concentration, it replaces Fe^{3+} ions at octahedral sites thereby decreasing super-exchange interactions and increasing magnetic dipolar interaction among these ions[38]. These results also support to the magnetization data reported in earlier work[22] which explain that there is weakening of super-exchange interactions with Ca^{2+} ions substitution as Ca^{2+} ions are entering octahedral sites replacing Fe^{3+} ions. In future, these samples will be used as sensing electrodes for chemical sensor application.

4 Conclusions

The pure and Ca doped $MgCa_xFe_{2-x}O_4$ ferrites of composition (x = 0.00, 0.01, 0.03, 0.05, 0.07) bulk samples structural and cations distribution details were derived by performing Rietveld refinement at recorded XRD patterns. These studies confirmed the partial inverse structure of the pure and Ca^{2+} ions doped Mg ferrite analogues. The doping of Ca^{2+} ions take place only at the octahedral sites. The values of cell parameters calculated by Rietveld refinement increases with calcium doping follows Vegard's law while density decreases. The increase in the lattice parameter is attributed to large ionic radius of calcium ions occupying octahedral sites. The stretching vibrational modes of Fe^{3+}– O^2 bond in the IR transmittance spectra are observed at ~ 600 cm^{-1} (ν_1)

of tetrahedral group and ~ 400 cm^{-1} (ν_2) of octahedral group respectively. The difference in the appearance of peak positions at these two sites is attributed to the difference in the Fe^{3+}– O^{2-} force constants at octahedral and tetrahedral sites. These peak positions are also composition dependent due to the variation in force constants by dopant ions substitution at octahedral sites. The splitting of ν_2 absorption band reveals the presence of cations of different characters on the same site. The ferromagnetic EPR spectra broadens with Ca^{2+} ions substitution in pure Mg – ferrite as evidenced from ΔH_{pp} values due to the spin disorder (frustrations) emerging from the antiferromagnetic interactions between the neighboring spins in the magnetic grains. The strong magnetic dipolar interaction enhances the lattice disorder. EPR parameters derived from recorded spectra also supports our earlier reported magnetization studies in which we discussed the weakening of super-exchange interactions on Ca^{2+} ions substitution and acquire both tetrahedral and octahedral sites by replacing Fe^{3+} ions.

Acknowledgements

One of the author (GK) is thankful to the Department of Physics, University of Jammu, Jammu for research support.

Conflict of Interest

The authors declare no conflict of interest

References

1 Singh N K, Singh S K, Dash D, Purkayastha B P, Joy J K & Maiti P J, *J Mater Chem*, 22 (2012) 1756.
2 Mohammed K A, Al–Rawas A D, Gismelseed A M, Sellai A, Widatallah H M, Yousif A, Elzain, M E & Shongwe M, *Physica B: Condens Matter J*, 407 (2012) 795.
3 Poddar P, Srikanth H, Morrison S A & Carpenter E E, *J Magn Magn Mater*, 288 (2005) 443.
4 Kikukawa N, Takemori M, Nagano Y, Sugasawa M & Kobayashi S, *J Magn Magn Mater*, 284 (2004) 206.
5 Goldman A, Modern Ferrite Technology, 2nd Edn, Springer Science Business Media Inc, New York (2006).
6 Khalaf K A M, Al – Rawas A D, Widatallah H M, Al – Rashdi K S, Sellai A, Gismelseed A M, Hashim Mohd., Jameel S K, Al – Raqeishi M S, Al – Riyami K O, Shongwe M & Al – Rajhi A H, *J Alloys Compd*, 657 (2016) 733.
7 Smit J & Wijn H P J, Ferrites Cleaver – Hume Press London U.K (1959).
8 Pradhan S K, Sumanta S & Dutta H, *Int Schol Res Net*, ISRN Ceramics, Article ID 194575 (2011), doi: 10.5402/ 2011/194575.
9 Grimes N W, Hilleard R J, Waters J & Yerkess J, *J Phys C*, 1 (1968) 663.
10 Bacon G E & Roberts F F, *Acta Crystal*, 6 (1953) 57.
11 Catra D, Casuala M F, Falqui A, Loche D, Mountjoy G, Sangregorio C & Corrias A, *J Phys Chem C*, 113 (2009) 8606.
12 Zakaria A K M, Abgar M A, Eriksson S G, Ahmed F U, Yunus S M, Delaplane R, Staliu V & Svedlindle V P, *Mater Res Bull*, 39 (2004) 1141.
13 Zakaria A K M, Abgar M A, Eriksson S G, Ahmed F U, Yunus S M & Rundlof H, *J Magn Magn Mater*, 265 (2003) 311.
14 Hossain S, Dev G, Aktar M S, Hassan M K, Zakaria A K M, Datta T K, Kamal I & Yunus, S M, *Am J Anal Chem*, 7 (2016) 203.
15 Sabri K, Rais A, Taibi K, Moreau M, Ouddane B & Addou A, *Physica B: Condens Matter J* , 501 (2016) 38.
16 Hemeda O M, *Turk J Phys*, 28 (2004) 121.
17 Patange S M, Shirsath S E, Jangam G S, Lohar K S, Jadhav S S, & Jadhav K M, *J Appl Phys*, 109 (2011) 053909.
18 Dhole V V, Khirade P P, Kale C M, Pandit V G, Shinde N D & Jadhav K M, *Int J Innovat Sci Eng Technol*, 2(2) (2015) 387.
19 Joshi H H & Kulkarni R G, J Mater Sci, 21 (1986) 2138.
20 Upadhyay R V & Kulkarni R G, *Mater Res Bull*, 19 (1984) 655.
21 Chhaya S D, Pandya M P, Chhantbar M C, Modi K B, Baldha G J & Joshi H H, *J Alloys Compd*, 377 (2004) 155.
22 Bamzai K K, Kour G, Kaur B & Kulkarni S D, *J Mater Sci*, 2014 (2014).
23 Brand R A, Georges-Gilbert H, Hubsch J L & Heller J A, *J Phys F Met Phys*, 15 (1985) 1987.
24 Jani N N, Trivedi B S, Joshi H H, Bichile G K & Kulkarni R G, *Bull Mater Sci*, 21 (1998) 233.
25 Modi K B, Joshi H H & Kulkarni R G, *J Mater Sci*, 31 (1996) 1311.
26 Bamzai K K, Kour G, Kaur B & Kulkarni S D, *J Magn Magn Mater*, 327 (2013) 159.
27 Bamzai K K, Kour G, Kaur B, Arora M & Pant R P, *J Magn Magn Mater*, 345 (2013) 255.
28 Waldron R D, *Phys Rev*, 99 (1955) 1727.
29 Srinivasan T T, Srivastava C M, Venkataramani N & Patni M J, *Bull Mater Sci*, 6 (1984) 1063.
30 Parmar V G, Modi K B & Joshi H H, *Indian J Pure Appl Phys*, 37 (1999) 207.
31 Iyer R, Desai R & Upadhyay R V, *Indian J Pure Appl Phys*, 47 (2009) 180.
32 Kotnala R K, Shah J, Singh B, Kishan H, Singh S, Dhawan S K & Sengupta A, *Sens Actuators B*, 129 (2008) 909.
33 Mazen S A, Abdallah M H, Sabrah B A & Hashem H A M, *Phys Stat Sol A*, 134 (1992) 263.
34 Silva P, Sagredo V, Bramer W, Perez E & Torres F, *J Phys: Conf Ser*, 200 (2010) 082023.
35 Eissa N A, Sallam H A, Salah S H, Mira A F & Hassib A, *Hyperfine Interact*, 28 (1986) 843.
36 Shah J, Arora M, Purohit L P & Kotnala R K, *Sens Actuators A*, 167 (2011) 332.
37 Gabal M A, *J Mater Sci*, 40 (2005) 387.
38 Baldha G J, Upadhyay R V & Kulkarni R G, *J Mater Sci*, 23 (1988) 3357.
39 Rodriguez – Carvajal J, Short Reference Guide of the FullProf Prog. Version 3.5 Laboratory Leon Brilloium (CEA – CNRS) (1997).

40 Knock H & Dannheim H, *Phys Stat Sol A*, 37 (1976) K135.
41 Blasse G, *Phillips Res Rep*, 3 (1964) l.
42 Hill R J, Craig J R & Gibbs G V, *Phys Chem Miner*, 4 (1979) 317.
43 Barth T F W & Posnjak E, Z Krist-New Cryst ST, 82 (1932) 325.
44 Chandradass J, Jadhav A H, Kim K H & Kim H, *J Alloys Compd*, 517 (2012) 164.
45 Reddy P V & Salagram M, *Phys Stat Sol A*, 100 (1987) 639.
46 Mazen S, Abdullah M H, Nakhla R I, Zaki H M & Metawe F, *J Mater Chem Phys*, 34 (1993) 35.
47 Dhole V V, Khirade P P, Kale C M, Patil V G, Shinde N D & Jadhav K M, *Int J Innovat Sci Eng Technol*, 2 (2015) 387.
48 Bhatu S S, Lakhani V K, Tanna A R, Vasoya N H, Buch J U, Sharma P U, Trivedi U N, Joshi H H & Modi K B, *Indian J Pure Appl Phys*, 45 (2007) 596.
49 Chhantbar M C, Trivedi U N, Tanna P V, Shah H J, Vara R P, Joshi H H & Modi K B, *Indian J Phys*, 78A (2004) 321.
50 Pasnicu C, Condurache D, Luca E, *Phys Stat Sol A*, 76 (1983) 145.
51 Khot S S, Shinde N S, Ladgaonkar B, Kale B B & Watawe S C, *Int J Adv Eng Technol*, 1 (2011) 422.
52 Dixit G, Singh J P, Srivastava R C & Agrawal H M, *J Magn Magn Mater*, 324 (2012) 479.
53 Luo Z, *EPR Studies of Hydrogenated Amorphous Silicon*, (1990).
54 Koseoglu Y & Aktas B, *Phys Stat Sol C*, 1 (2004) 3516.
55 Koseoglu Y, Burucu O, Kumru M, Yildiz F, Rana M U & Aktas B, *Proc 3rd Moscow Int Symp Magn*, 261 (2005).
56 Vanhaelst M & Claijw P, *Phys Stat Sol B*, 87 (1978) 719.
57 Kurikka V, Shafi P M, Koltypin Y & Gedanken A, *J Phys Chem B*, 101 (1997) 6409.
58 Upadhyay R V, Srinivas D & Mehta R V, *J Magn Magn Mater*, 214 (2000) 105.